Local Grid Refinement in New Zealand's Earth System Model: Tasman Sea Ocean Circulation Improvements and Super-Gyre Circulation Implications

Erik Behrens[1], Jonny Williams[1], Olaf Morgenstern[1], Phil Sutton[12], Graham Rickard[1], Mike Williams[1]

[1]National Institute for Water and Atmospheric Research (NIWA), 301 Evans Bay Parade, Hataitai, Wellington 6021, New Zealand

[2] School of Environment, University of Auckland, New Zealand

Corresponding author: Erik Behrens (erik.behrens@niwa.co.nz)

Key Points:

- NZESM is a nested fully coupled ESM based on UKESM with a high-resolution ocean grid of 1/5° around New Zealand
- The oceanic circulation is improved in NZESM over the nested domain and model biases of temperature and salinity are reduced
- The Super-Gyre intensifies and expands southward due to wind changes triggered by changes in the large-scale heat transport

Abstract

This paper describes the development of New Zealand's Earth System Model (NZESM) and evaluates its performance against its parent model (United Kingdom Earth System Model, UKESM) and observations. The main difference between the two earth system models is an embedded high-resolution (1/5°) nested region over the oceans around New Zealand in the NZESM. Due to this finer ocean model mesh, boundary currents such as the East Australian Current, East Australian Current Extension, Tasman Front and Tasman Leakage and their transports are better simulated in NZESM. The improved oceanic transports have led to a reduction in upper ocean temperature and salinity biases over the nested region. In addition, net transports through the Tasman Sea of volume, heat and salt in the NZESM agree better with previously reported estimates. A consequence of the increased cross-Tasman transports in the NZESM is increased temperatures and salinity west of Australia and in the Southern Ocean reducing the meridional sea surface temperature gradient between subtropics and sub-Antarctic. This also leads to a weakening of the westerly winds between 60°S and 45°S over large parts of the Southern Ocean, which reduces the northward Ekman transport, reduces the formation of Antarctic Intermediate Water and allows for a southward expansion of the Super-Gyre in all ocean basins. Connecting an improved oceanic circulation around New Zealand to a basin-wide Super-Gyre response is an important step forward in our current understanding of how local scales can influence global scales in a fully coupled earth system model.

Plain Language Summary

We describe the model development of the New Zealand Earth System Model and assess its performance against the model on which it is based (United Kingdom Earth System Model) and observations. The New Zealand Earth System Model is a fully coupled earth system model, which aims to model all relevant bio-physical processes in and between the atmosphere, land, ocean and sea-ice. The main difference between the both models is that the oceans around New Zealand in the New Zealand Earth System Model are more precisely modelled, due to a refined ocean model mesh in this region. That results in a more accurate oceanic circulation around New Zealand in the New Zealand Earth System Model compared to the United Kingdom Earth System Model and reduced model biases of temperature and salinity. These oceanic changes have implications beyond the oceans around New Zealand and cause a warming in the Southern Ocean and a related weakening of the westerly winds over the Southern Ocean. This weakening of the winds allows subtropical waters to reach further in the Southern Ocean. It is notable how regional changes in the ocean circulation can have implications on the global scale.

1 Introduction

New Zealand is a maritime continent and its weather and climate are directly impacted by the surrounding ocean (Basher and Thompson 1996; Mullan 1998). It occupies the interface between subtropical waters to its north and sub-Antarctic water masses to its south, separated by the Subtropical Front (STF). Due to the prevailing westerly winds, the Tasman Sea and the air-sea fluxes of heat and moisture over this region can be considered a pacemaker for New Zealand's weather and climate. The Tasman Sea is fuelled by the East Australian Current (EAC), which transports warm and salty waters from the tropics along the east coast of Australia into the Tasman Sea (Figure 1b). At around 32°S the EAC bifurcates into the EAC-Extension (EAC-Ext), which continues southward, and the Tasman Front (TF), which flows eastward towards New Zealand. Whether or not the name TF is appropriate for this flow, or if it is better described

as an eastern extension of the EAC-Ext is currently under debate (Oke et al. 2019). The EAC-Ext is a region of high mesoscale eddy activity with eddies transporting water from the boundary current into the interior Tasman Sea (Bull et al. 2017; Oliver, O'Kane, and Holbrook 2015). A portion of the EAC-Ext leaves the Tasman Sea as Tasman Leakage (TL) to the Indian Ocean (Speich et al. 2002; Rintoul and Bullister 1999). This export pathway is part of the Super-Gyre circulation, which connects all three subtropical gyres in the Southern Hemisphere (Cai 2006). The TF crosses the Tasman Sea and feeds the East Auckland Current (EAUC); the western boundary current on the east coast of the North Island of New Zealand. This current continues south and interacts with a series of standing eddies before following the Chatham Rise into the Pacific Ocean (Chiswell et al. 2015).

The STF is located at around 45°S south of Tasmania and is characterised by strong horizontal gradients in temperature, salinity and nutrients (Orsi, Whitworth, and Nowlin 1995). A weak eastward flow is associated with the STF while crossing the Tasman Sea. The STF is deflected south as it approaches the South Island of New Zealand. The STF forms the Southland Current east of the South Island and then turns east along Chatham Rise.

The interaction of these currents and water masses with the exceptional bathymetry, such as sea-mounts, ridges and plateaus around New Zealand, make the oceanic conditions unique and challenging to model and to observe. Long-term oceanographic observations in the region include mooring arrays within the EAC, Expandable Bathythermograph transects between New Zealand, Australia and Fiji and dispersed Argo data. Glider missions within the EAC and EAUC are slowly complementing our understanding of variability of these boundary currents.

Global climate models struggle to precisely simulate the oceanic conditions in this region (Rickard, Behrens, and Chiswell 2016; Law et al. 2017), which has motivated tailored model development such as ACCESS-OM (Bi et al. 2013). Some of the reported model biases of these coupled models can be linked to the relatively coarse oceanic model grids and the models not being able to precisely simulate western boundary currents and cannot resolve important processes such as mesoscale eddies. To overcome this shortcoming some modelling centres have developed high-resolution configurations for CMIP6 (e.g. Storkey et al. (2018)) to incorporate the impact of mesoscale eddies. Such global high-resolution simulations have been shown to reduce some model biases (Roberts et al. 2016; Muller et al. 2018), at the expense of computational cost, which restricts the number of applications and simulations. Nested model grids provide an alternative, where areas of interest can be simulated at finer scales and at much lower computational cost. In this paper we describe such a tailored model solution for New Zealand which, together with other model developments, has become known as the New Zealand Earth System Model (NZESM).

The paper is structured as follows. Section 3 provides the model description of NZESM. Section 4 highlights the model performance of NZESM against the United Kingdom Earth System Model (UKESM) and observations and section 5 provides a discussion and summary.

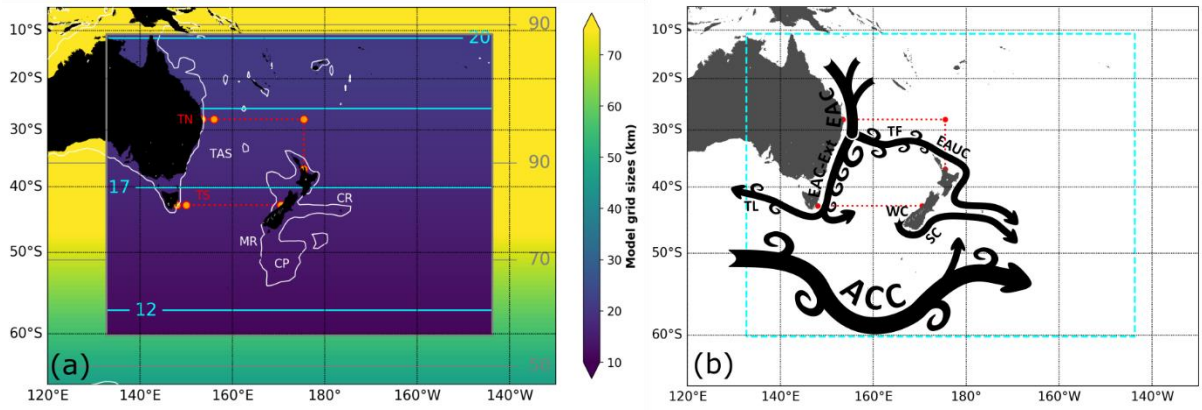

Figure 1. (a) Grid sizes of NZESM in km with high-resolution domain embedded into a global eORCA1 domain. Two control sections which run from Australia to New Zealand are shown in red dots. The orange dots mark the segments which have been used to calculate transports. The Macquarie Ridge (MR), Campbell Plateau (CP), Chatham Rise (CR), and Tasman Sea (TAS), Tasman North (TN) section and Tasman South (TS) section have been labelled. The 1000m iso-bath is show by the white contour line. (b) Schematic of major ocean currents in the region: East Australian Current (EAC), East Australian Current Extension (EAC-Ext), Tasman Front (TF), East Auckland Current (EAUC), Westland Current (WC), Southland Current (SC), Antarctic Circumpolar Current (ACC).

2 Model description

NZESM is based on UKESM (see (Kuhlbrodt et al. 2018; Storkey et al. 2018; Sellar et al.) for details. NEMO (Madec 2008) is used to simulate the ocean physics, CICE (Hunke et al. 2017; Rae et al. 2015) for sea-ice, the Unified Model (UM) (Walters et al. 2019) for the atmosphere, JULES (Walters et al. 2019) for the land surface and MEDUSA (Yool, Popova, and Anderson 2013) for ocean-biogeochemistry. All model components are coupled together via OASIS-MCT (Craig, Valcke, and Coquart 2017) to build a fully-coupled interactive earth system model (ESM).

NEMO supports local grid refinement capabilities, also known as nesting (Adaptive Grid Refinement In Fortran, AGRIF (Debreu, Vouland, and Blayo 2008)). Here a fine model mesh can be embedded in a coarser ocean model grid via a two-way nesting scheme, allowing for interactive coupling between both model grids. Several nested configurations have been established in the past to address scientific research questions (Behrens 2013; Behrens et al. 2012; Biastoch, Bning, and Lutjeharms 2008; Schwarzkopf et al. 2019). In the case of NZESM the nested high-resolution ocean model domain spans from 132.7°E to 143.7°W and 60.17°S to 10.75°S with a nominal resolution of 1/5°, which translates into grids sizes of 12km to 20km (Figure 1a); this resolution makes the model eddy-permitting around New Zealand. The vertical grid, identical between both model grids, uses 75 z-levels, with a 1m surface layer which increases with depth to up to 200m in thickness. The model background viscosity and diffusivity for the nested region have been set to bi-Laplacian 5×10^{10} and 200 respectively, in comparison to 200 and 1000 for the global grid. The time step of the nested domain has been reduced to 900s compared to 2700s for the global model. For compatibility reasons with AGRIF, a linear-free surface has been used instead of a fully-free surface as in UKESM. In addition, a climatology of iceberg-related meltwater fluxes, based on UKESM, has been applied instead of the Lagrangian iceberg tracking scheme, due to the incompatibility of the latter with AGRIF. Apart from these two differences the model settings are identical to UKESM. The model results in section 4 show that differences between NZESM and UKESM originate from the presence of the high-resolution

nest and can be causally linked together. Therefore, we assume that the other differences have a minor impact on the model response.
In this version of NZESM, the coupling with the atmospheric model is accomplished via the global coarse model, which contains the upscaled information of the nested region.
The atmospheric model therefore does not experience the directly-resolved eddy fluxes of the nested grid.
For this model comparison paper, we use the historical simulations from UKESM and NZESM covering the period from 1950-2014, with NZESM initialised with the same start dump of UKESM in 1950. We note that grid refinement has been applied to NEMO to improve ocean physics in the nested region, but not to MEDUSA. However, improvements to the ocean physics (e.g. ocean circulation) due to the high-resolution nest will impact MEDUSA on the coarser global grid. These bio-geochemical impacts are out of scope for this work and will be assessed separately.
Modelled temperature and salinity has been compared with results from the shorter time series (2004-2018) Roemmich–Gilson Argo climatology [*Roemmich and Gilson*, 2009]. The Roemmich–Gilson product consists of optimally-interpolated Argo profiles on a 1° × 1° grid of longitude and latitude and can be downloaded from http://sio-argo.ucsd.edu/RG_Climatology.html. The monthly Argo-derived temperature values extend over 58 pressure levels from the surface to 2000m depth. Remotely-sensed absolute dynamic topography (ADT), a multi-mission altimeter product (Ssalto/Duacs) from Archiving, Validation and Interpretation of Satellite Oceanographic data (AVISO) has been compared to modelled sea surface height (SSH) to characterize near surface circulation and variability. The Ssalto/Duacs altimeter products were produced and distributed by the Copernicus Marine and Environment Monitoring Service (http://www.marine.copernicus.eu).

3 Model results

3.1 Mean SSH and variance field

The mean Sea Surface Height (SSH) fields from AVISO, UKESM and NZESM are shown in Figure 2a-c. In AVISO the EAC, the EAC-Ext and the TF are clearly represented by compressed contour lines, which reflect strong geostrophic currents. The horizontal gradient over the Tasman Sea is weak, although there is flow associated with the STF in the order of 3 Sv (Stramma, Peterson, and Tomczak 1995). But since it is largely density compensated it is not characterised by a large SSH gradient. To the east of New Zealand's North Island, the southward flow associated with the EAUC and East Cape Currents can be seen, with SSH contours turning southward towards the Chatham Rise. South of 50°S the influence of the Antarctic Circumpolar Current (ACC) is visible with large SSH gradients reflecting strong surface currents. The northern portion of the ACC is deflected southward by the presence of the Campbell Plateau, before the flow turns northward towards the Chatham Rise, east of the Campbell Plateau.

The mean SSH pattern of UKESM does capture the large-scale features seen in AVISO. The EAC and EAC-Ext are too wide and the bifurcation of the EAC into the EAC-Ext and the TF is too far south. The circulation east of New Zealand is reasonably well captured; however, the flow in the ACC is too strong and too zonal compared to AVISO and tends to expand too far northwards to the east of the Campbell Plateau.

The SSH pattern of NZESM is more in agreement with AVISO than UKESM. The width of the EAC is similar to that in AVISO and the flow pattern of the TF across the Tasman Sea matches AVISO. Flows associated with the ACC now show the meridional diversions as seen in AVISO, west and east of the Campbell Plateau. The ACC itself is stronger than in UKESM in some regions, which could be a result of a more realistic and steeper bathymetry in NZESM. The bathymetry in UKESM is smoother, allowing flows to extend over larger regions, compared to steeper bathymetry where flows become concentrated and intensified.

SSH variance provides an indirect measure for eddy kinetic energy and is shown in Figure 2d-f. AVISO exhibits large variability within the EAC, the separation region and the EAC-Ext. The variability quickly decays away from the Australian coast. Enhanced variability is also present in the ACC, especially in regions where the ACC shows large meridional variability. In UKESM none of this eddy variability is present due to the coarse model grid, which does not allow for mesoscale eddies to be resolved. NZESM, on the other hand, produces a similar SSH variance pattern to AVISO. Large eddy variability is present in the EAC region, particularly near the region where the EAC separates into the EAC-Ext and the TF. NZESM also shows enhanced eddy variability within the same regions of the ACC as AVISO. The NZESM intensity in the sub-Antarctic is slightly higher than in AVISO, while the intensities agree well within the EAC separation region. But north of the separation region variability is too low in the model.

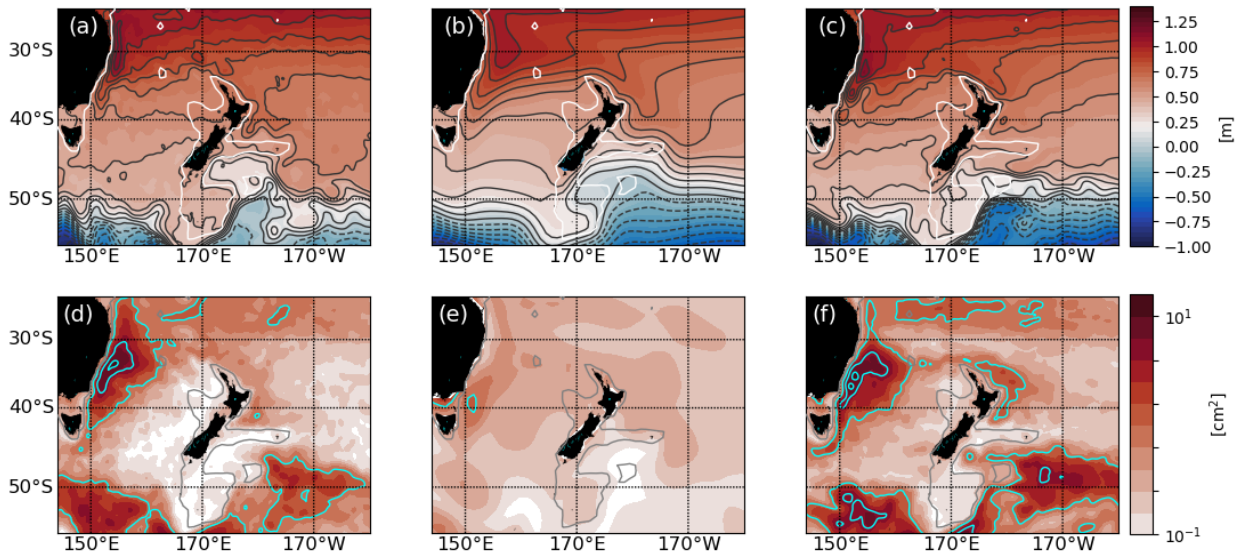

Figure 2. Mean (1995-2014) SSH fields for (a) AVISO, (b) UKESM and (c) NZESM. Contour interval for SSH (black contour lines) is 10cm. The 1000m iso-bath is show by the white/grey contour line. Variance of SSH for AVISO (d), UKESM (e) and NZESM (f). Contour levels for SSH variance (light blue lines) are 1, 5, 10, and 15cm^2.

3.2. Mean cross-section properties along Tasman North

In the following section we describe the differences between UKESM and NZESM across two sections which bound the Tasman Sea (Figure 1a). The Tasman North (TN) section cuts through the warm water pathway into the Tasman Sea running across 28°S from Australia to 178°E

before turning south with an end point near Auckland. Along the zonal part of this section it crosses the EAUC.

The UKESM and NZESM temperature fields are similar (Figure 3a,d); warmest water is found near Australia as part of the EAC inflow and the temperatures become colder moving east along the TN section. The difference between NZESM and UKESM shows that temperatures in NZESM are about 0.5°C warmer in the top 250m, except for the EAC. Below 500m temperatures in NZESM are in general around 0.5° colder than UKESM, except near the boundaries where temperatures up to 1°C warmer. In NZESM the heat transport of the EAC (below 100m) and EAUC are larger than in UKESM and cause the positive anomalies near both coasts and in the top 250m along the northern boundary of the TF.

The salinity field shows three different vertical layers (Figure 3b,e), with high salinity values in the top 500m, which is linked water with subtropical origin. Below this is a fresh layer between 500m and 1250m of AAIW, with saltier waters underneath associated with Pacific Deep Waters (PDW). The difference between NZESM and UKESM highlights that salinity in NZESM is in general fresher in the upper 1250m, except for the boundary currents and PDW layer, which are saltier. This freshening, together with the negative cold anomaly at this similar depth range, could imply a strengthening of the AAIW formation south of New Zealand. However, results at the Tasman South (TS) section promote a different explanation and point to changes in the circulation and heat transport within the Subtropical Gyre, which will be discussed in section 3.7.

The cross-section velocities show that with increasing model resolution the boundary currents become narrower and more intense. The EAC extends up to 500km off the coast in UKESM, while in NZESM it is only 250km. The same behavior is visible for the EAUC and in the difference between NZESM-UKESM (Figure 3i).

The differences in temperature and salinity seen along the section can be mainly explained by changes in the cross-Tasman transports, the EAC and the TF. UKESM shows a very weak southward transport through the Tasman of around -0.93 Sv, which is lower than observations suggest (Table 1). NZESM with a net southward transport of -4.82 Sv sits within the range of earlier reported values of around -3 Sv to -9 Sv. Overall the transport values of the EAC, the TF and the EAC-Ext in NZESM are closer to the observed values than in UKESM, which overestimates the TF transport by a factor of two.

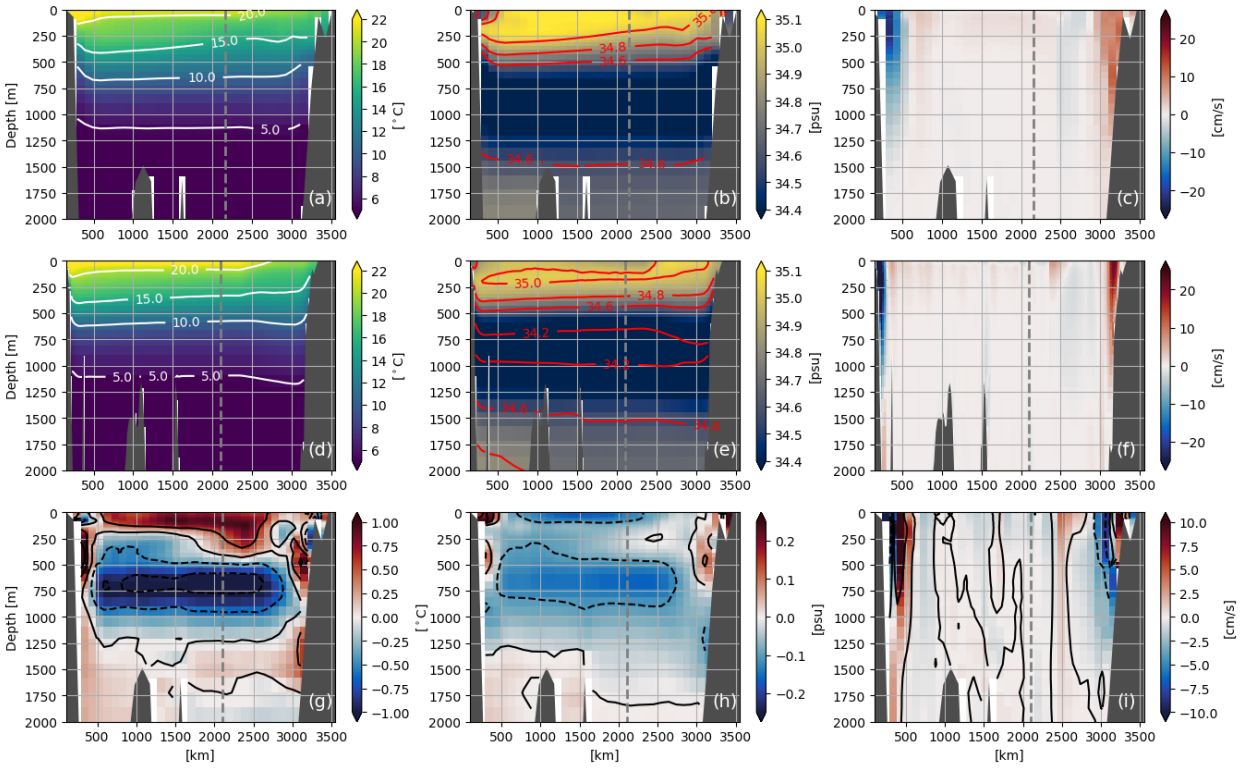

Figure 3. Mean properties (1995-2014) along the Tasman North section. (a,d) Temperature, (b,e) salinity and (c-f) cross-section velocity for UKESM (top row) and NZESM (middle row). The difference (NZESM minus UKESM) is shown in the bottom row. Temperature contour interval is 5°C. The contour interval for salinity is 0.2 psu. The grey dashed line marks the point where the section turns from zonal to meridional. Contour interval for temperature difference is 0.5°C, for salinity 0.1 psu and 5 cm/s for cross-section velocities.

	Observations	UKESM	NZESM
EAC volume	-25 to -37 Sv (Ridgway and Dunn 2003) -22 (Mata et al. 2000) -22 (Sloyan et al. 2016)	-28.7 Sv	-16.8 Sv
EAC-Ext volume	-19 Sv (Ridgway and Dunn 2003)	-7.1 Sv	-8.8 Sv
TF volume	13 Sv (Ridgway and Dunn 2003) 8 (Stanton 2010)	21.8 Sv	9.5 Sv
TL volume	-8 Sv (Rintoul and Sokolov 2001) -8 Sv (Ridgway and Dunn 2007a)	-8.0 Sv	-10.6 Sv
Cross-Tasman volume	-7.4 Sv (Ridgway and Dunn 2003) -9 Sv (Ridgway and Godfrey 1994) -3 to -8 Sv (Hill et al. 2011)	-0.33	-4.82
Cross-Tasman Heat		-24×10^{12} J/s	-320×10^{12} J/s
Cross-Tasman FW		0.01 Sv	-0.07 Sv
ITF	15 Sv (Gordon et al. 2010)	15.3 Sv	14.8 Sv

STG Pacific Ocean 153°E to 173°E, 37.5°S to 20°S		-43.9 Sv	-45.4 Sv
STG Indian Ocean 23°W to 53°W, 45°S to 20S°	-41 to -58 Sv(Palmer et al. 2004)	-94.1 Sv	-96.6 Sv
STG Atlantic Ocean -57°W to 27°W, 45°S to 20S°		-49.5 Sv	-51.3 Sv

Table 1. Time mean (1995-2014) transports.

3.3. Mean cross-section properties along Tasman South

Along the TS section the impact of changes in cross-Tasman transports between UKESM and NZESM is more obvious (Figure 4a,d). Here NZESM is substantially warmer over the entire section, with differences reaching up to 2°C (Figure 4g) in the top 750m in the central Tasman Sea. This is due to the combined impact of EAC-Ext eddies being resolved in NZESM, which carry warm and salty waters from the boundary current (EAC-Ext) into the interior Tasman Sea, and the enhanced southward cross-Tasman transport in NZESM. Between 1000m and 1250m positive temperature anomalies are present, which are opposite to the TN section at this depth range.

The salinity differences in the top 750m are very coherent to the temperature differences, with salinity being up to 0.5 psu saltier in NZESM compared to UKESM. This supports our conclusion about the increased southward volume, heat and salt transport and a more unstable EAC-Ext in NZESM. However, the AAIW layer becomes fresher (750m-1750m), which can be a consequence of an enhanced AAIW production or a surface freshening in the formation region. We can rule out an enhanced AAIW production since it conflicts with the positive temperature differences at this depth range. Therefore, that suggests that a freshening in the Southern Ocean and a weakening of the AAIW production are the reasons for this negative salinity anomaly. That is further supported by diagnostics in section 3.7.

In UKESM the EAC-Ext and the TL extend up to 750km into the Tasman Sea, compared with only 250km in NZESM. In general, NZESM shows more meridional structures than UKESM over the section. Near the New Zealand shelf a southward flow is visible, the Westland Current, which contributes to the STF. This current is more prominent and wider in NZESM and barely recognisable in UKESM.

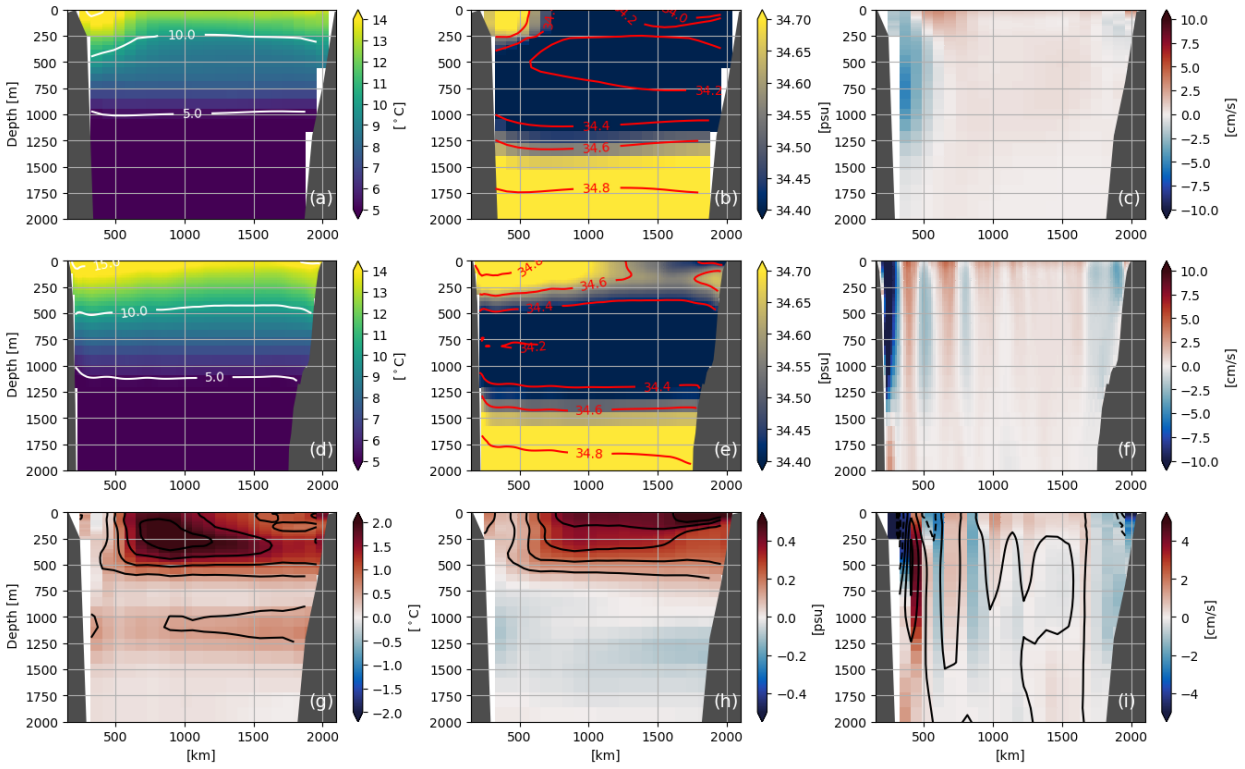

Figure 4. Mean properties (1995-2014) along the Tasman South section. (a,d) Temperature, (b,e) salinity and (c-f) cross-section velocity for UKESM (top row) and NZESM (middle row). The difference between NZESM minus UKESM is shown in the bottom row. Temperature contour interval is 5°C. The contour interval for salinity is 0.2 psu. Contour interval for temperature difference is 0.5°C, for salinity 0.1 psu and 5 cm/s for cross-section velocities.

3.4. Mean properties in the Tasman Sea

The TN and TS sections enclose a large portion of the Tasman Sea, which we use to investigate the mean temperature and salinity profiles against Argo, shown in Figure 5 for the upper 1000m where the differences are largest. The mean profiles for the Tasman Sea are shown by the solid lines, and the shading indicates the minimum and maximum over the period 2004-2014.

For temperature in the top 50 m, UKESM is around 1°C cooler compared to the Argo mean profile and the minimum values. Here NZESM shows a better match with Argo with only small differences. Between 100m and 600m NZESM is around 0.8 °C cooler than Argo, while UKESM shows a close match with Argo.

Salinity in both models are too fresh compared to Argo. Differences reach up to 0.8 psu in the upper 200m of the water column and decrease to 0.2 psu at 1000m. In NZESM the salt bias is reduced in the top 700m by around 0.2 psu. UKESM shows a large range of around ±0.2 psu within the top 200m, while the range of Argo and NZESM is smaller around ±0.1 psu. The reasons for the overall fresh bias of both models is connected the general precipitation surplus compared to observations over most of the Pacific and Indian Ocean (Sellar et al.). However, overall NZESM shows improvement in the temperature (salinity) in the top 100m (700m) compared to UKESM.

The temporal variability of these temperature and salinity profiles is shown in Figure 6 and Figure 7, where the seasonal cycle of UKESM has been removed from all datasets. UKESM shows a positive temperature trend over the entire period of about 1.2°C/decade (top 1000m), in-

line with the increasing CO_2 concentrations. The largest warming occurs in the top 400m of the water column. This same layer also has the largest interannual variability of around ±0.5 °C. The temperature trend in NZESM is very similar to UKESM. The largest warming and transient adjustment from the UKESM state occurs within the first 10 years, with a warming of around 0.5°C in the top 1000m intensified at around 400m depth compared to UKESM. Not only does the mean temperature differ between UKESM and NZESM but also the interannual to decadal variability, while both show the similar warming trend.

Salinity in UKESM (Figure 7a) shows two opposing trends. The top 600m becomes saltier (0.1 psu/decade), while the layer between 600-1000m becomes fresher (-0.06 psu/decade). The salinity in NZESM adjusts within the first 10 years from the UKESM state as for temperature. The top 100m shows the largest salinity increase by about 0.2 psu which decreases with depth. Only little change is seen below 800m, with freshening trends in NZESM slightly larger (-0.13 psu/decade) for 600-1000m than in UKESM.

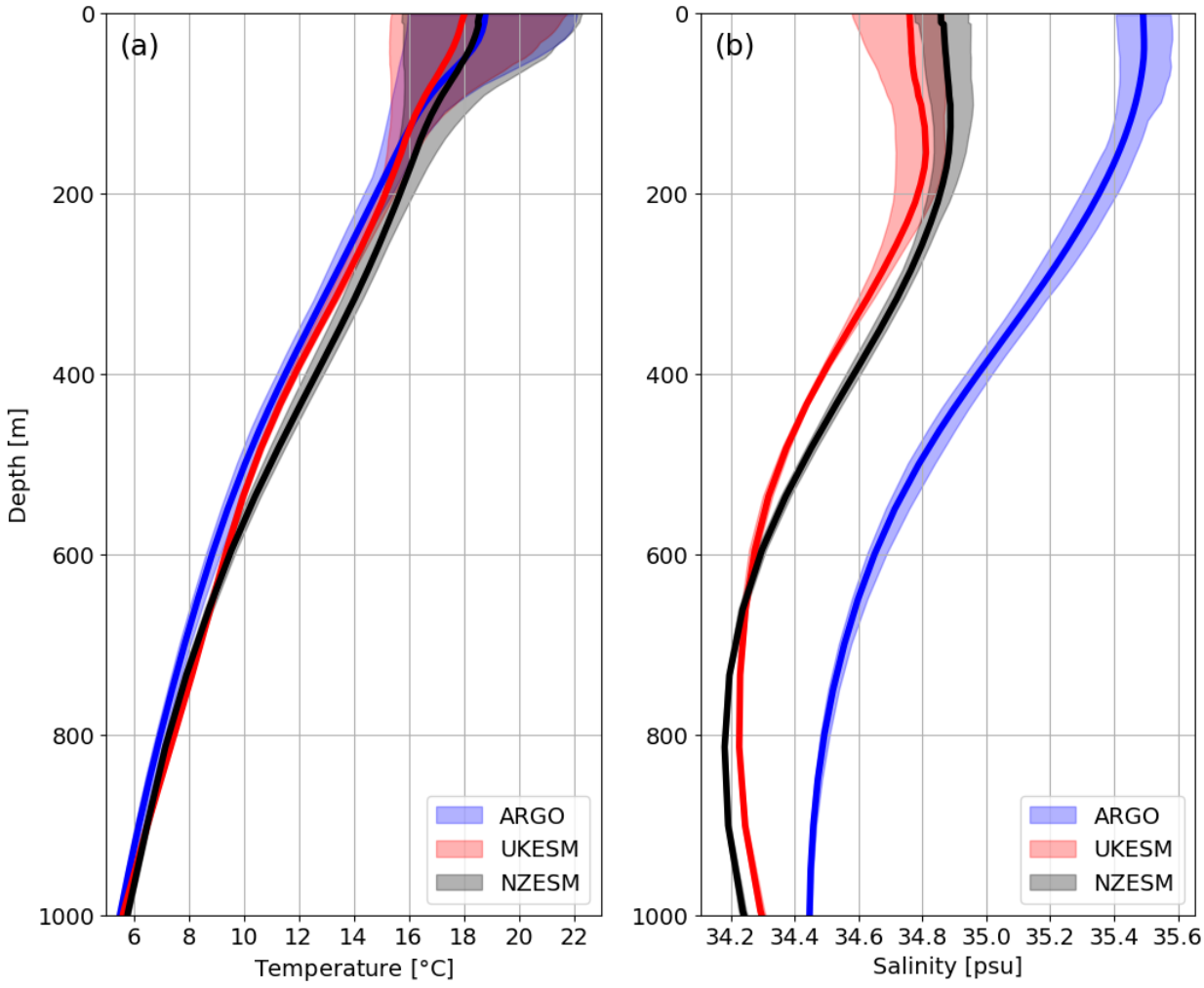

Figure 5. Vertical mean (2004-2014) profiles for (a) temperature, (b) salinity in the Tasman Sea.

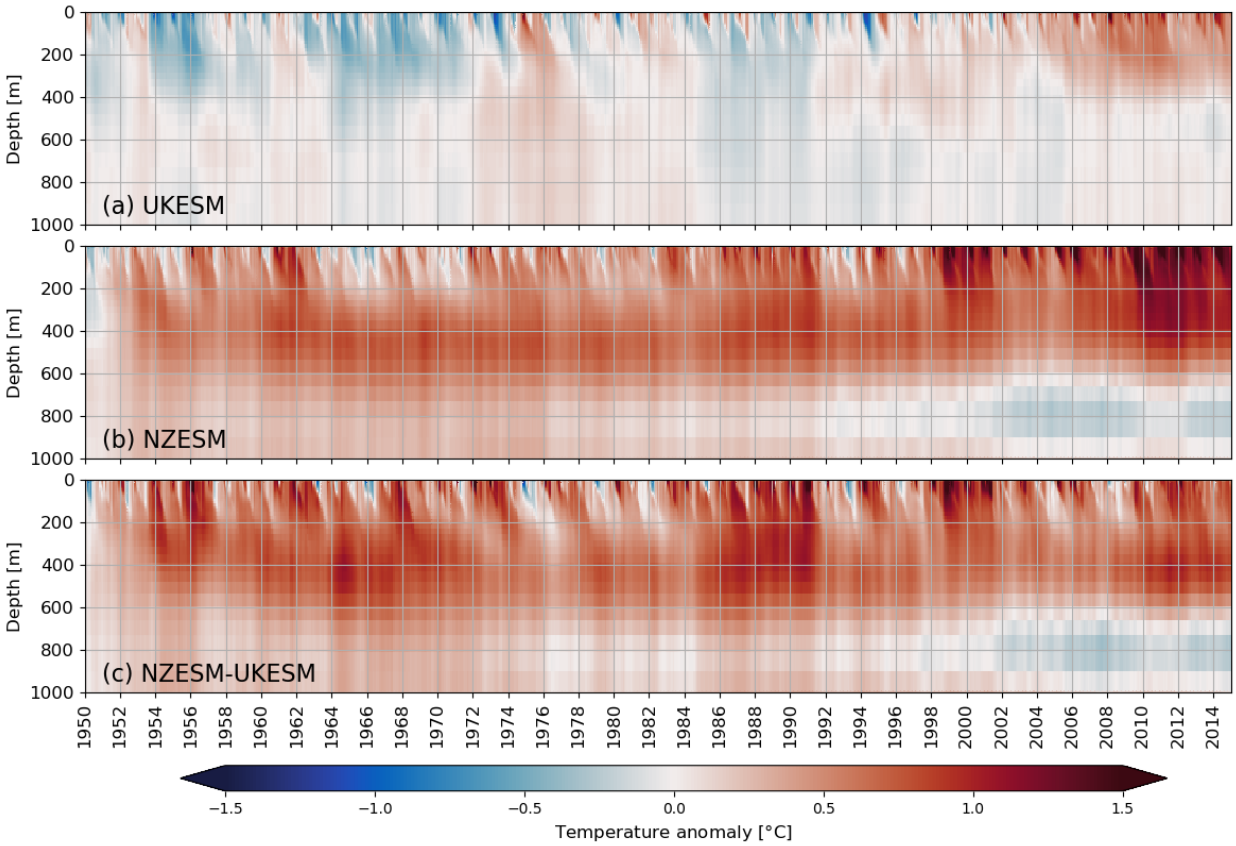

Figure 6. Temporal evolution of the mean temperature anomalies in the Tasman Sea for (a) UKESM, (b) NZESM and (c) NZESM minus UKESM. The seasonal cycle from UKESM has been subtracted.

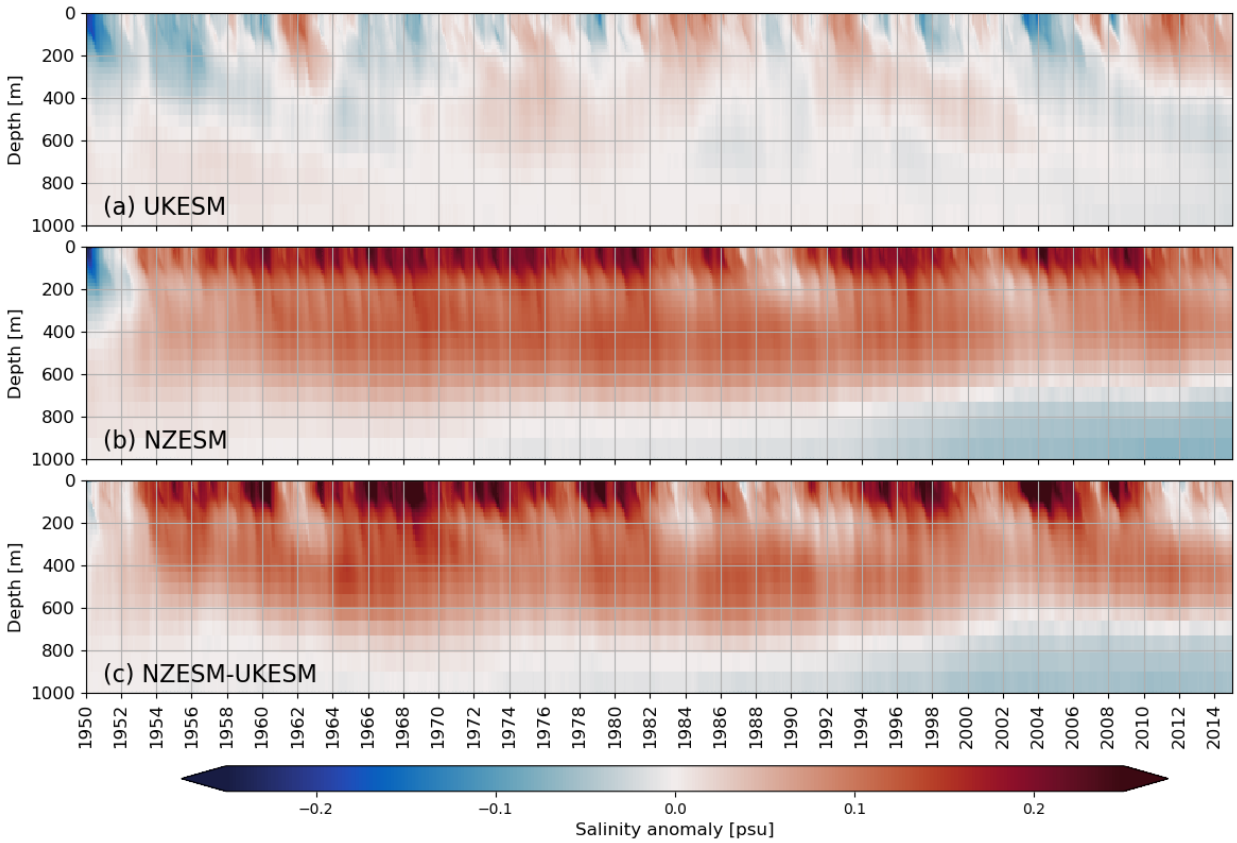

Figure 7. Temporal evolution of the mean salinity anomalies over the Tasman Sea for (a) UKESM, (b) NZESM and (c) NZESM minus UKESM. The seasonal cycle of UKESM has been subtracted.

3.5 Surface temperature and salinity biases

After having presented the localised impacts on the Tasman Sea, we show the regional changes due to the presence of the high-resolution nest in NZESM. Since the Argo climatology does not cover high-latitudes (<60°S) we use EN4 (Good, Martin, and Rayner 2013) as a reference. This dataset is widely used to assess the model performance (Storkey et al. 2018). Surface temperature and salinity biases of UKESM and NZESM are shown in Figure 8. UKESM shows a general cold bias exceeding -0.5°C north of ~35°S. The EAC-Ext is too warm, while the remaining Tasman Sea is more than -1°C too cold. East of New Zealand we observe a dipole pattern with a positive bias north east of the Chatham Rise and a negative bias south east of it. In the ACC region the biases tend to be positive, with biases exceeding 2°C east of 150°E. In comparison to UKESM, in NZESM the cold model bias north of New Zealand is reduced. The Tasman Sea changes from a large negative to small positive model bias in the order of 0.2°C. In addition, the model biases east of New Zealand have also been reduced in NZESM in size and intensity. The only region where model biases have become larger are in the Australian sector south of 50°S, where previously positive biases of 0.5°C now exceed 1.5°C. This warming is consistent with the temperature anomalies shown across the TS section, Figure 4.
UKESM has an overall negative surface salinity bias in the subtropical region. The SSS bias exceeds -1.5 psu around 10°S, 160°W. The negative bias becomes weaker when moving south until it turns positive between 55°S and 60°S. Over the Tasman Sea the bias is between -0.6 to -

0.7 psu. In NZESM the fresh bias is reduced in most regions and values in the Tasman Sea are close to -0.5 psu, while values along the TN section have increased slightly.

Some of the changes in the model biases between UKESM and NZESM can be attributed to changes in the oceanic circulation in NZESM. As presented earlier, NZESM transports more heat into and through the Tasman Sea, which results in warmer SSTs and reduces the overall negative SST bias in this region. In combination with an enhanced salt transport into and through the Tasman Sea in NZESM, the warmer SST increases evaporation which causes a further reduction of the negative SSS bias.

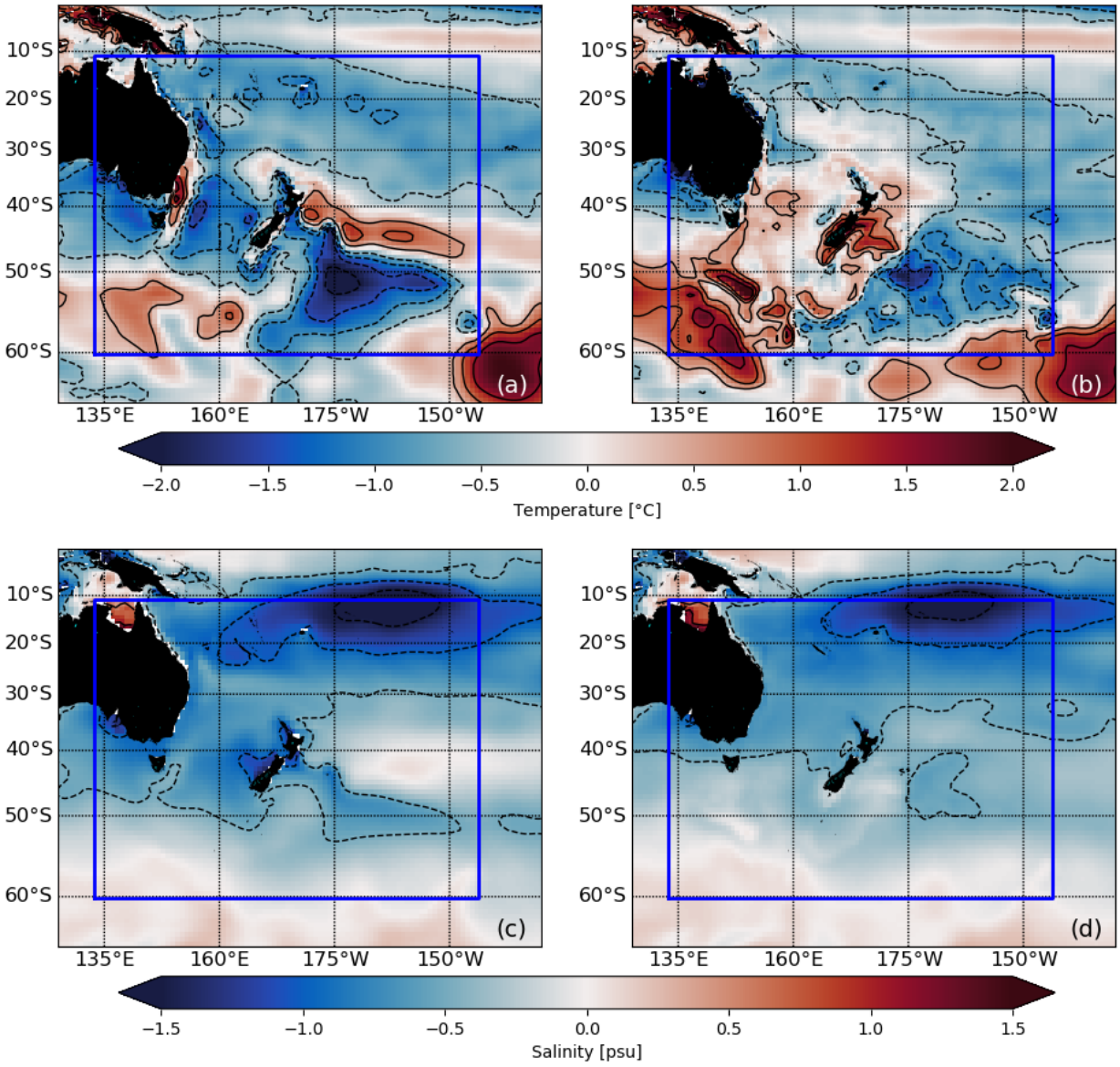

Figure 8: Surface model biases 1995-2014, compared to EN4. (a) SST UKESM, (b) SST NZESM, (c) SSS UKESM and (d) SSS NZESM. The dark-red box marks the region of the high-resolution nest. Contour interval for temperature is 0.5°C and 0.5psu for salinity.

3.6 Advective response of top 500m temperature and salinity anomalies

In this section we seek to highlight the advective response of the nested region in NZESM, due to changes in volume, heat and freshwater transports. These changes, in combination with atmospheric feedbacks, trigger responses far beyond the boundaries of the nested high-resolution domain. Here we present the mean temperature and salinity differences over the top 500m between NZESM and UKESM (Figure 9). In these depth-averaged differences, the response due to ocean advection is dominant over changes in the surface fluxes of heat and freshwater.
The largest impact occurs inside the boundaries of the nested region, confirming that differences between NZESM and UKESM are mainly driven by the presence of the high-resolution nest in NZESM. In NZESM the Tasman Sea is around 1.5°C warmer compared to UKESM. This anomaly extends into the Indian Ocean sector between 60°S and 40°S, over the Chatham Rise and south east into the Southern Ocean. To the east of the Chatham Rise a large negative anomaly has developed exceeding 2°C, which extends further into the Pacific Ocean.
The main anomaly pattern can be attributed to the changes in the oceanic circulation in NZESM. As described in sections 4.2 and 4.3, the southward cross-Tasman transport of heat is increased in NZESM compared to UKESM. This change in heat advection between NZESM and UKESM causes the positive temperature difference in the Tasman Sea, the south Indian Ocean and the Chatham Rise. In UKESM most of this heat is carried instead through the Tasman Sea by the overly strong TF to the east of New Zealand. In NZESM this heat pathway is reduced due to a more realistic transport of the TF and causes the negative anomalies in this region. The positive temperature differences west of Australia are a result of the increased TL transport of heat and feeds into the northern branch of the Indian Subtropical Gyre (van Sebille et al. 2012).
Salinity shows a very similar difference pattern to temperature, where positive differences span from the Tasman Sea into the South Indian and South Pacific Ocean. The good match to the temperature differences suggest that most of these anomalies are caused by changes in the ocean advection of heat and freshwater, rather than by regional changes in the surface fluxes.

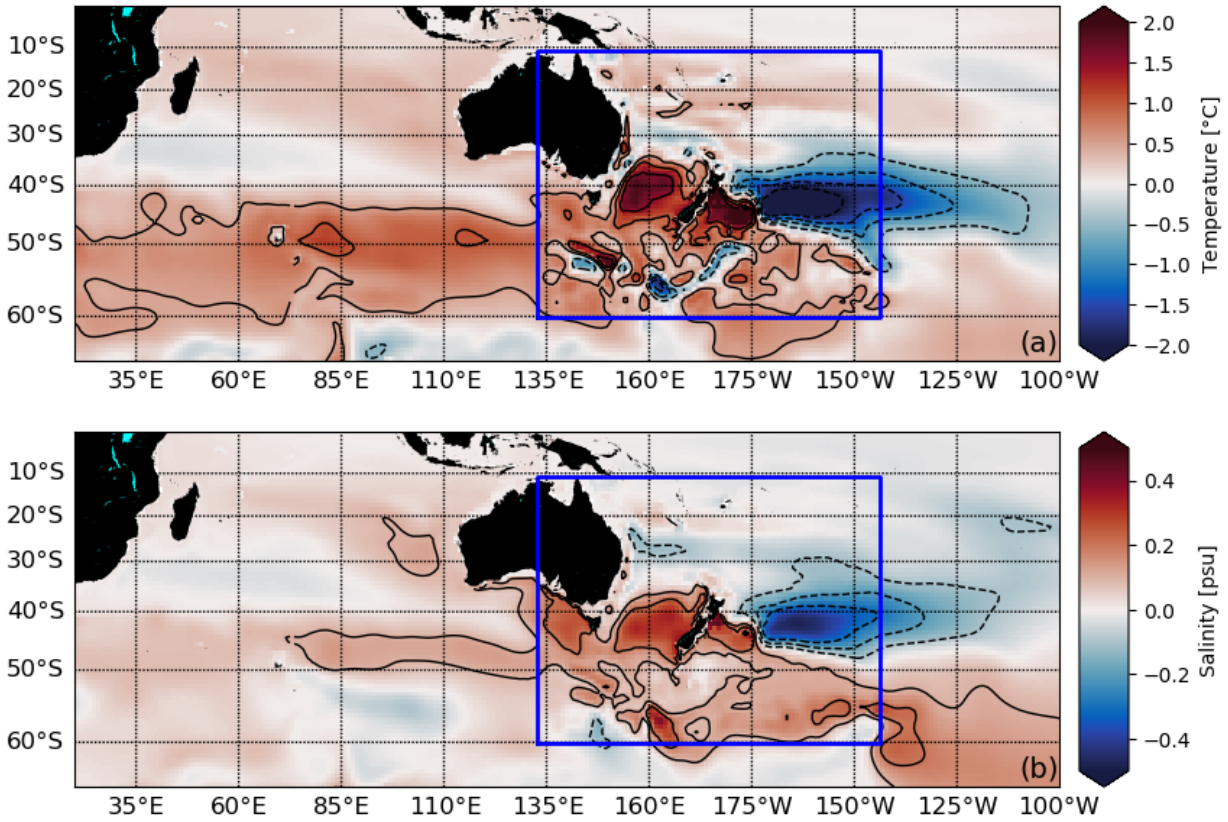

Figure 9. Mean (1995-2014) top 500m (a) temperature and (b) salinity difference: NZESM minus UKESM. The dark-red box marks the region of the high-resolution nest. Contour interval for temperature is 0.5°C and 0.5psu for salinity.

3.7 Impacts on the Super-Gyre circulation

As seen in the previous sections, the differences are not restricted to the nested regions and have far reaching impacts due to advective processes and atmospheric feedbacks. This can impact the basin-scale circulation including the Super-Gyre circulation, which connects all three subtropical gyres in the southern hemisphere (Cai 2006; Ridgway and Dunn 2007b; Speich, Blanke, and Cai 2007). The barotropic streamfunction for UKESM, NZESM and the difference is shown in Figure 10, highlighting the Super-Gyre circulation and the inter-basin connectivity. The 0 Sv contour is shown for UKESM and NZESM to define the gyre boundaries. All three subtropical gyres are visible in UKESM and NZESM, with centres near the western boundary due to the western intensification. The barotropic streamfunction difference shows a strengthening for all three gyres centres of between 2-4 Sv (see Table 1). Over the nested region we see a weakening of the circulation north of New Zealand (positive anomalies) of about 8 Sv, which reflects weaker transports of the TF in NZESM compared to UKESM. This large-scale weakening in combination with changes in the heat transport explains the negative temperature anomalies in the TN section at depths between 500m and 1000m and are not driven by changes in the AAIW formation. Along the Campbell Plateau and along the Chatham Rise we see enhanced circulation, which is reflected by negative (positive) anomalies north (south) of the Super-Gyre boundary.

In addition to the enhanced Super-Gyre circulation, a slight southward expansion of the gyre boundary is visible in most regions in the Southern Ocean. The southward expansion is caused by reduced zonal wind stress south of the Super-Gyre boundary between 60°S and 45°S of about 5%-10% (Figure 11) in NZESM compared to UKESM. The exception is the Indian Ocean sector where zonal winds increase. The overall reduction in zonal winds leads to a weakening of northward Ekman transport and allows for a southward expansion of the Super-Gyre. The reduction in Ekman transport causes a weakening of AAIW formation, which was seen in the TS section (section 4.3 and Figure 4) by positive temperature anomalies in the AAIW depth range (1000-1250m). The related slightly negative salinity anomalies suggest in addition a freshening of the source waters, which is supported by the negative anomalies in Figure 9 around 60°S - 65°S south of Australia and New Zealand.

Lastly, the intensification of the individual subtropical gyre transports is due to positive wind stress curl anomalies over the gyre centres (Figure 12) on the western side of each basin. This results in a speed up of gyre circulation in each basin via the Sverdrup circulation.

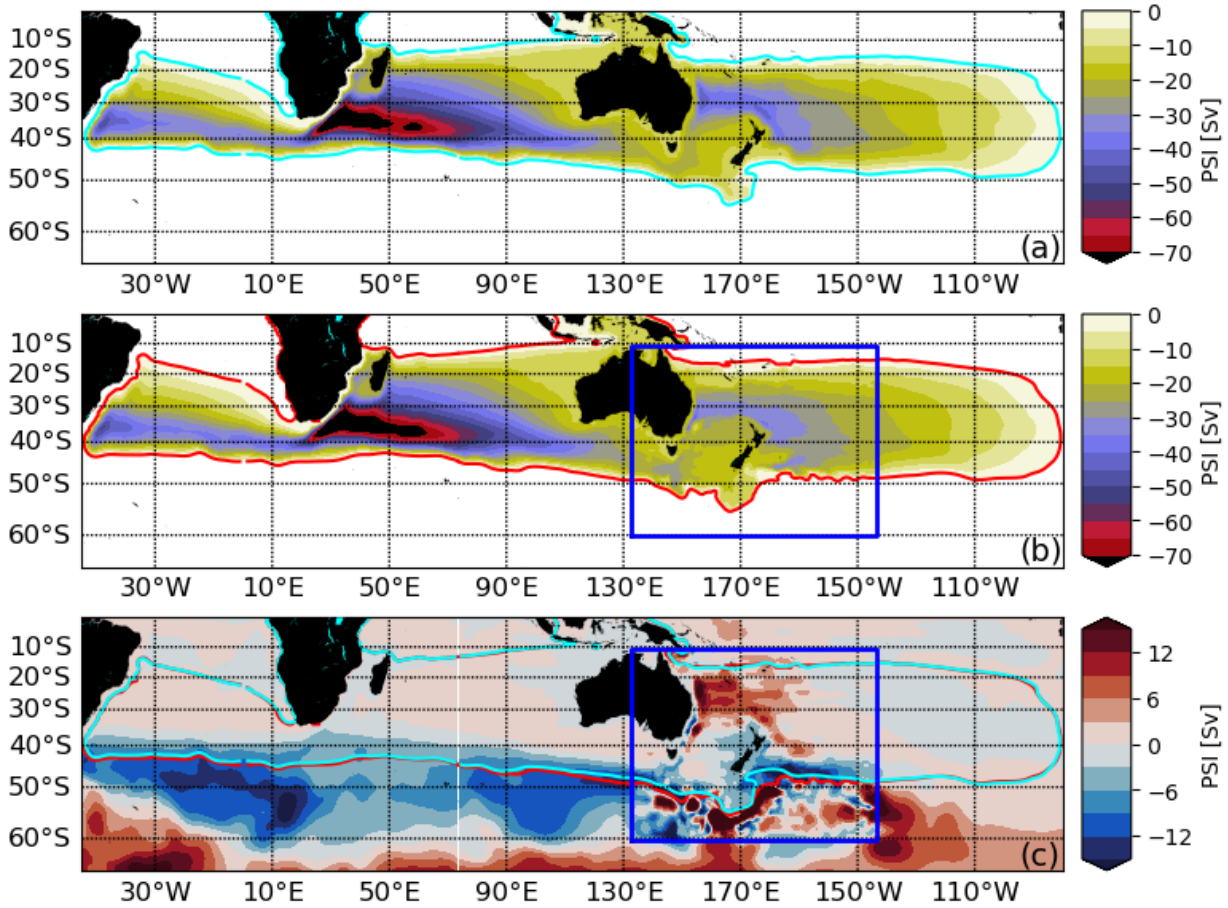

Figure 10. Time mean (1995-2014) barotropic stream function for (a) UKESM and (b) NZESM and (c) difference (NZESM minus UKESM). Blue (red) contour shows 0 Sv contour for UKESM (NZESM). The nested region is shown by the blue box.

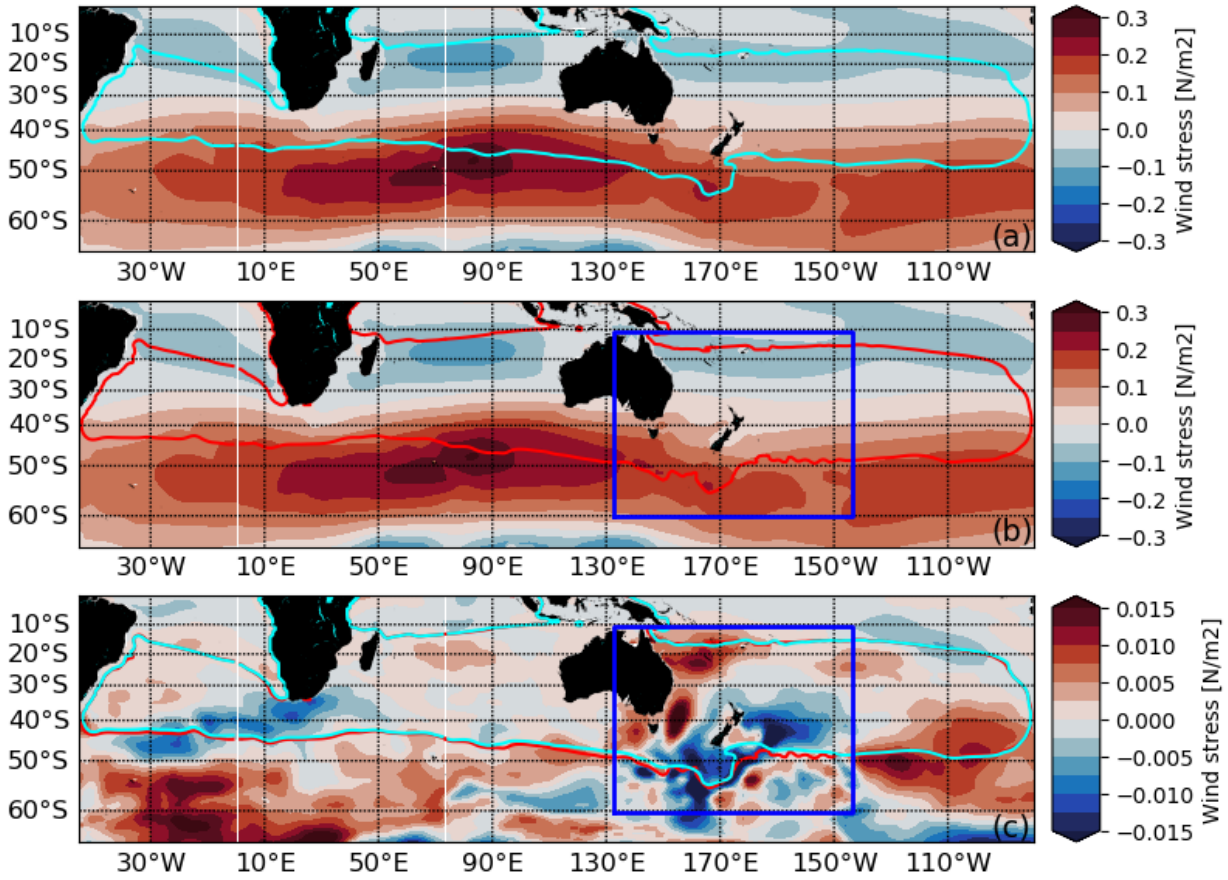

Figure 11. Time mean (1995-2014) zonal wind stress (a) UKESM and (b) NZESM and (c) difference between NZESM minus UKESM. The nested region is shown by the red box. The zero Sverdrup contour line of the barotropic streamfunction of UKESM (cyan) and NZESM (red) is overlaid. The nested region is shown by the dark-red box.

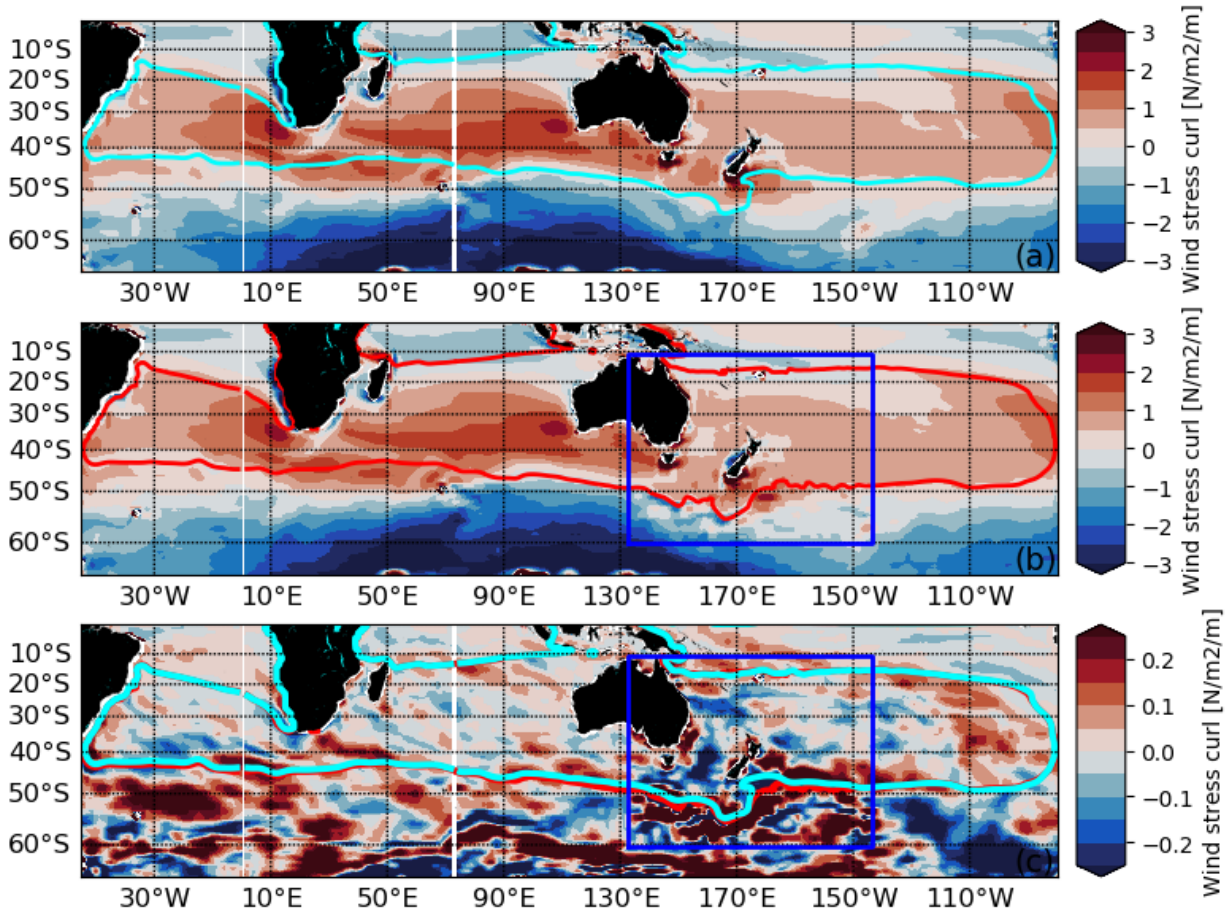

Figure 12. Time mean (1995-2014) wind stress curl for (a) UKESM and (b) NZESM and (c) difference between NZESM minus UKESM. Values have been scaled by 1×10^{7}. The nested region is shown by the red box. The zero Sverdrup contour line of the barotropic streamfunction of UKESM (cyan) and NZESM (red) is overlaid. The nested region is shown by the black box.

4. Conclusions and Discussion

NZESM is a fully coupled earth system model based on UKESM (Kuhlbrodt et al. 2018). This paper describes the model development of NZESM and evaluates its model performance against UKESM and observations. The main enhancement of NZESM compared with UKESM is an embedded high-resolution (1/5°) nested ocean around New Zealand. This has been accomplished through local grid refinement techniques using AGRIF (Debreu, Vouland, and Blayo 2008) with a two-way nesting scheme, which allows for a smooth transition of signals between the nested grid and the global coarse 1° ocean grid.

The comparison between NZESM, UKESM and observations shows that, due to the finer model mesh in NZESM, the oceanic circulation in the nested region has been improved compared to UKESM. Volume transports of the EAC, EAC-Ext, TF and TL in NZESM agree better with observed values. Here, UKESM overestimates transports of the EAC and TF by up to a factor of two and underestimates transport of the EAC-Ext. Transports of these currents in NZESM do not differ more than 15% from the observed values. This improvement is mainly achieved through a better representation of the boundary currents, which are too wide in UKESM, and a more

realistic bifurcation of the EAC into the EAC-Ext and TL. Here mesoscale eddies play an important role and NZESM simulates the eddy field in the bifurcation region better than UKESM.

The improved separation into the EAC-Ext and TL in NZESM has consequences for the cross-Tasman transport. In UKESM the net volume, heat and salt transport through the Tasman Sea is too low compared to previous estimates. In NZESM these transports are within the range of those estimates and lead to a reduction of model biases in temperature and salinity in this region. UKESM shows a large-scale cold (~1-2°C) and fresh (~0.7 psu) bias at the surface around New Zealand. These biases are reduced to nearly zero (±0.2°C) for temperature and ~0.5 psu for salinity. Since the temperature biases are small and do not show a similar pattern to the fresh biases, we conclude that an excess of precipitation and not a lack of evaporation is the main cause for the remaining fresh bias. Reasons remain unknown and are beyond the scope of this ocean-focused study.

Due to ocean advection and atmospheric feedbacks in combination with the two-way nesting, the impact of the high-resolution region propagates well beyond the nest boundaries. The enhanced transport of heat and salt within the TL and through the Tasman Sea cause temperature and salinity to increase along the west coast of Australia and in the upper 500m of the Southern Ocean.

The SST increase has atmospheric implications too, since it reduces the large-scale meridional SST gradient between subtropical and subpolar regions. That, in turn, weakens the westerlies following the thermal wind equation. This weakening of westerlies is observed in a meridional band between 45°S to 60°S and reduces the northward Ekman transport and causes the Super-Gyre to extend further into the Southern Ocean.

The southward extension has also been recognised in UKESM when comparing the low-resolution version, based on a global 1° (eORCA1) ocean grid, with a high-resolution version based on a global 0.25° (eORCA025) ocean grid (Sellar et al.). These results confirm our hypothesis and findings that the expansion is related to the improved transports of the boundary currents, as seen in NZESM. However, the expansion of the Super-Gyre in UKESM (eORCA025) results in larger SST and sea-ice biases in the Southern Ocean compared with the lower resolution (eORCA1) configurations. In this respect, the performance of UKESM (eORCA1) is better due to a cancellation of errors, which is to some extent linked to the impact of mesoscale eddies in this region. The UKESM (eORCA025) model grid does not resolve them fully in the Southern Ocean, while they are parametrized in the UKESM (eORCA1) configuration. Trying to shed light into the impact of eddies in the Southern Ocean and their regional impact is an active and complex field of research (Hogg et al. 2013; Meredith 2016; Doddridge et al. 2019) and nesting provides a potential way forward (Patara, Boening, and Biastoch 2016) to improve our understanding.

The Super-Gyre expansion in NZESM goes along with a gyre circulation intensification of around 2-4 Sv, as a consequence of increased wind-stress curl over the individual subtropical gyre centres via the Sverdrup balance. Both the expansion and extension of the Super-Gyre have various ramifications; such as the transport of salt from the Indian to the Atlantic Ocean via the Agulhas Leakage. This has far-reaching consequences for the Atlantic Meridional Overturning Circulation as well as the circulation and sea-ice in the Southern Ocean. Although we observe changes in those quantities, causal links all the way from oceanic changes around New Zealand beyond the Super-Gyre scale are not trivial to establish and are beyond the scope of this paper.

The bio-geochemical implications of improvements in the ocean physics around New Zealand are also excluded here.

Nevertheless, we have demonstrated with the development of NZESM that we can reduce model biases around New Zealand by embedding a high-resolution ocean nest in a global, relatively coarse resolution earth system model, with a feasible computational cost to allow for a sequence of simulations. Therefore, the oceanic circulation around New Zealand is more precisely captured in NZESM than without this high-resolution focal region in UKESM. Due to this step forward, we speculate that climate projections and climate variability modelled by NZESM will be more precise and accurate than without this tailored model development for the New Zealand region.

Acknowledgments

This paper obtained funding and support through the Ministry of Business Innovation and Employment Deep South National Science Challenge projects (C01X1412) and Royal Society Marsden Fund (NIW1701). We would like to acknowledge the NeSI High Performance Computing Facility team for their technical support. In addition, we would like to acknowledge the technical guidance of Jérôme Chanut (IPSL, France), Pat Hyder (MetOffice, UK), Jan Harlaβ (GEOMAR, Germany), Torge Martin (GEOMAR, Germany) and the support of Frances Boyson and my son with this project.

The model output of NZESM (u-bl274 MetOffice identifier) and UKESM (u-bm456 MetOffice identifier) used for the manuscript is publicly available via Zenodo (http://doi.org/10.5281/zenodo.3581390 and http://doi.org/10.5281/zenodo.3581410) respectively. The model code for NZESM (NEMO+CICE) is publicly available from https://github.com/erikbehrens/NZESM1 .

References

Basher, R. E., and C. S. Thompson. 1996. 'Relationship of air temperatures in New Zealand to regional anomalies in sea-surface temperature and atmospheric circulation', *International Journal of Climatology*, 16: 405-25.

Behrens, Erik. 2013. "The oceanic response to Greenland melting: the effect of increasing model resolution." Christian-Albrechts University Kiel.

Behrens, Erik, Franziska U. Schwarzkopf, Joke F. Lbbecke, and Claus W. Bning. 2012. 'Model simulations on the long-term dispersal of 137 Cs released into the Pacific Ocean off Fukushima', *Environmental Research Letters*, 7: 034004.

Bi, D. H., S. J. Marsland, P. Uotila, S. O'Farrell, R. Fiedler, A. Sullivan, S. M. Griffies, X. B. Zhou, and A. C. Hirst. 2013. 'ACCESS-OM: the ocean and sea-ice core of the ACCESS coupled model', *Australian Meteorological and Oceanographic Journal*, 63: 213-32.

Biastoch, Arne, Claus W. Bning, and Johan R. E. Lutjeharms. 2008. 'Agulhas leakage dynamics affects decadal variability in Atlantic overturning circulation.', *Nature*, 456: 489--92.

Bull, Christopher Y. S., Andrew E. Kiss, Nicolas C. Jourdain, Matthew H. England, and Erik van Sebille. 2017. 'Wind Forced Variability in Eddy Formation, Eddy Shedding, and the Separation of the East Australian Current', *Journal of Geophysical Research: Oceans*, 122: 9980--98.

Cai, W. 2006. 'Antarctic ozone depletion causes an intensification of the Southern Ocean super-gyre circulation', *Geophysical Research Letters*, 33: L03712.

Chiswell, Stephen M., Helen C. Bostock, Philip J. H. Sutton, and Michael J. M. Williams. 2015. 'Physical oceanography of the deep seas around New Zealand: a review', *New Zealand Journal of Marine and Freshwater Research*: 1--32.

Craig, A., S. Valcke, and L. Coquart. 2017. 'Development and performance of a new version of the OASIS coupler, OASIS3-MCT_3.0', *Geoscientific Model Development*, 10: 3297-308.

Debreu, Laurent, Christophe Vouland, and Eric Blayo. 2008. 'AGRIF: Adaptive grid refinement in Fortran', *Computers \& Geosciences*, 34: 8--13.

Doddridge, E. W., J. Marshall, H. Song, J. M. Campin, M. Kelley, and L. Nazarenko. 2019. 'Eddy Compensation Dampens Southern Ocean Sea Surface Temperature Response to Westerly Wind Trends', *Geophysical Research Letters*, 46: 4365-77.

Good, Simon A., Matthew J. Martin, and Nick A. Rayner. 2013. 'EN4: Quality controlled ocean temperature and salinity profiles and monthly objective analyses with uncertainty estimates', *Journal of Geophysical Research: Oceans*, 118: 6704--16.

Gordon, A. L., J. Sprintall, H. M. Van Aken, D. Susanto, S. Wijffels, R. Molcard, A. Ffield, W. Pranowo, and S. Wirasantosa. 2010. 'The Indonesian throughflow during 2004-2006 as observed by the INSTANT program', *Dynamics of Atmospheres and Oceans*, 50: 115-28.

Hill, K. L., S. R. Rintoul, K. R. Ridgway, and P. R. Oke. 2011. 'Decadal changes in the South Pacific western boundary current system revealed in observations and ocean state estimates', *Journal of Geophysical Research*, 116: C01009.

Hogg, Andrew McC, Michael P. Meredith, Don P. Chambers, E. Povl Abrahamsen, Chris W. Hughes, and Adele K. Morrison. 2013. 'Recent trends in the Southern Ocean eddy field', *Journal of Geophysical Research: Oceans*, 120: 257--67.

Hunke, Elizabeth, William Lipscomb, Philip Jones, Adrian Turner, Nicole Jeffery, and Scott Elliott. 2017. "CICE, The Los Alamos Sea Ice Model." In.

Kuhlbrodt, Till, Colin G. Jones, Alistair Sellar, Dave Storkey, Ed Blockley, Marc Stringer, Richard Hill, Tim Graham, Jeff Ridley, Adam Blaker, Daley Calvert, Dan Copsey, Richard Ellis, Helene Hewitt, Patrick Hyder, Sarah Ineson, Jane Mulcahy, Antony Siahaan, and Jeremy Walton. 2018. 'The Low-Resolution Version of HadGEM3 GC3.1: Development and Evaluation for Global Climate', *Journal of Advances in Modeling Earth Systems*, 10: 2865--88.

Law, Cliff S., Graham J. Rickard, Sara E. Mikaloff-Fletcher, Matt H. Pinkerton, Erik Behrens, Steve M. Chiswell, and Kim Currie. 2017. 'Climate change projections for the surface ocean around New Zealand', *New Zealand Journal of Marine and Freshwater Research*: 1--27.

Madec, Gurvan. 2008. 'NEMO the Ocean Engine', *Tech. Rep., Notes de l'IPSL*, 27: 193.

Mata, Mauricio M., Matthias Tomczak, Susan Wijffels, and John A. Church. 2000. 'East Australian Current volume transports at 30°S: Estimates from the World Ocean Circulation Experiment hydrographic sections PR11/P6 and the PCM3 current meter array', *Journal of Geophysical Research: Oceans*, 105: 28509--26.

Meredith, M. P. 2016. 'Understanding the structure of changes in the Southern Ocean eddy field', *Geophysical Research Letters*, 43: 5829-32.

Mullan, A. B. 1998. 'Southern hemisphere sea-surface temperatures and their contemporary and lag association with New Zealand temperature and precipitation', *International Journal of Climatology*, 18: 817-40.

Muller, W. A., J. H. Jungclaus, T. Mauritsen, J. Baehr, M. Bittner, R. Budich, F. Bunzel, M. Esch, R. Ghosh, H. Haak, T. Ilyina, T. Kleine, L. Kornblueh, H. Li, K. Modali, D. Notz, H. Pohlmann, E. Roeckner, I. Stemmler, F. Tian, and J. Marotzke. 2018. 'A Higher-resolution Version of the Max Planck Institute Earth System Model (MPI-ESM1.2-HR)', *Journal of Advances in Modeling Earth Systems*, 10: 1383-413.

Oke, P. R., G. S. Pilo, K. Ridgway, A. Kiss, and T. Rykova. 2019. 'A search for the Tasman Front', *Journal of Marine Systems*, 199.

Oliver, Eric C. J., Terence J. O'Kane, and Neil J. Holbrook. 2015. 'Projected changes to Tasman Sea eddies in a future climate', *Journal of Geophysical Research: Oceans*, 120: 7150--65.

Orsi, Alejandro H., Thomas Whitworth, and Worth D. Nowlin. 1995. 'On the meridional extent and fronts of the Antarctic Circumpolar Current', *Deep Sea Research Part I: Oceanographic Research Papers*, 42: 641--73.

Palmer, M. D., H. L. Bryden, J. Hirschi, and J. Marotzke. 2004. 'Observed changes in the South Indian Ocean gyre circulation, 1987-2002', *Geophysical Research Letters*, 31.

Patara, Lavinia, Claus W. Boening, and Arne Biastoch. 2016. 'Variability and trends in Southern Ocean eddy activity in 1/12° ocean model simulations', *Geophysical Research Letters*, 43: 4517--23.

Rae, J. G. L., H. T. Hewitt, A. B. Keen, J. K. Ridley, A. E. West, C. M. Harris, E. C. Hunke, and D. N. Walters. 2015. 'Development of the Global Sea Ice 6.0 CICE configuration for the Met Office Global Coupled model', *Geoscientific Model Development*, 8: 2221-30.

Rickard, Graham J., Erik Behrens, and Stephen M. Chiswell. 2016. 'CMIP5 earth system models with biogeochemistry: An assessment for the southwest Pacific Ocean', *Journal of Geophysical Research: Oceans*, 121: 7857--79.

588 Ridgway, K. R., and J. R. Dunn. 2003. 'Mesoscale structure of the mean East Australian Current System and its
589 relationship with topography', *Progress In Oceanography*, 56: 189-222.
590 ———. 2007a. 'Observational evidence for a Southern Hemisphere oceanic supergyre', *Geophysical Research*
591 *Letters*, 34.
592 Ridgway, K. R., and J. S. Godfrey. 1994. 'Mass and heat budgets in the East Australian current: A direct approach',
593 *Journal of Geophysical Research*, 99: 3231.
594 Ridgway, Ken R., and J. R. Dunn. 2007b. 'Observational evidence for a Southern Hemisphere oceanic supergyre',
595 *Geophysical Research Letters*, 34: n/a--n/a.
596 Rintoul, S. R., and J. L. Bullister. 1999. 'A late winter hydrographic section from Tasmania to Antarctica', *Deep-Sea*
597 *Research Part I-Oceanographic Research Papers*, 46: 1417-54.
598 Rintoul, Stephen R., and Serguei Sokolov. 2001. 'Baroclinic transport variability of the Antarctic Circumpolar
599 Current south of Australia (WOCE repeat section SR3)', *Journal of Geophysical Research: Oceans*, 106:
600 2815--32.
601 Roberts, M. J., H. T. Hewitt, P. Hyder, D. Ferreira, S. A. Josey, M. Mizielinski, and A. Shelly. 2016. 'Impact of
602 ocean resolution on coupled air-sea fluxes and large-scale climate', *Geophysical Research Letters*, 43:
603 10430-38.
604 Schwarzkopf, F. U., A. Biastoch, C. Boning, J. Chanut, J. V. Durgadoo, K. Getzlaff, J. Harlass, J. K. Rieck, C. Roth,
605 M. M. Scheinert, and R. Schubert. 2019. 'The INALT family - a set of high-resolution nests for the Agulhas
606 Current system within global NEMO ocean/sea-ice configurations', *Geoscientific Model Development*, 12:
607 3329-55.
608 Sellar, Alistair A., Colin G. Jones, Jane Mulcahy, Yongming Tang, Andrew Yool, Andy Wiltshire, Fiona M.
609 O'Connor, Marc Stringer, Richard Hill, Julien Palmieri, Stephanie Woodward, Lee de Mora, Till
610 Kuhlbrodt, Steve Rumbold, Douglas I. Kelley, Rich Ellis, Colin E. Johnson, Jeremy Walton, Nathan Luke
611 Abraham, Martin B. Andrews, Timothy Andrews, Alex T. Archibald, Ségolène Berthou, Eleanor Burke, Ed
612 Blockley, Ken Carslaw, Mohit Dalvi, John Edwards, Gerd A. Folberth, Nicola Gedney, Paul T. Griffiths,
613 Anna B. Harper, Maggie A. Hendry, Alan J. Hewitt, Ben Johnson, Andy Jones, Chris D. Jones, James
614 Keeble, Spencer Liddicoat, Olaf Morgenstern, Robert J. Parker, Valeriu Predoi, Eddy Robertson, Antony
615 Siahaan, Robin S. Smith, Ranjini Swaminathan, Matthew T. Woodhouse, Guang Zeng, and Mohamed
616 Zerroukat. 'UKESM1: Description and evaluation of the UK Earth System Model', *Journal of Advances in*
617 *Modeling Earth Systems*, n/a.
618 Sloyan, Bernadette M., Ken R. Ridgway, Rebecca Cowley, Bernadette M. Sloyan, Ken R. Ridgway, and Rebecca
619 Cowley. 2016. 'The East Australian Current and Property Transport at 27°S from 2012 to 2013', *Journal of*
620 *Physical Oceanography*, 46: 993--1008.
621 Speich, S., B. Blanke, and W. J. Cai. 2007. 'Atlantic meridional overturning circulation and the Southern
622 Hemisphere supergyre', *Geophysical Research Letters*, 34.
623 Speich, Sabrina, Bruno Blanke, Pedro de Vries, Sybren Drijfhout, Kristofer Ds, Alexandre Ganachaud, and Robert
624 Marsh. 2002. 'Tasman leakage: A new route in the global ocean conveyor belt', *Geophysical Research*
625 *Letters*, 29: 55--1--55--4.
626 Stanton, B. R. 2010. 'An oceanographic survey of the Tasman Front', *New Zealand Journal of Marine and*
627 *Freshwater Research*, 15: 289--97.
628 Storkey, D., A. T. Blaker, P. Mathiot, A. Megann, Y. Aksenov, E. W. Blockley, D. Calvert, T. Graham, H. T.
629 Hewitt, P. Hyder, T. Kuhlbrodt, J. G. L. Rae, and B. Sinha. 2018. 'UK Global Ocean GO6 and GO7: a
630 traceable hierarchy of model resolutions', *Geoscientific Model Development*, 11: 3187-213.
631 Stramma, L., R. G. Peterson, and M. Tomczak. 1995. 'The South-Pacific Current', *Journal of Physical*
632 *Oceanography*, 25: 77-91.
633 van Sebille, Erik, Matthew H. England, Jan D. Zika, and Bernadette M. Sloyan. 2012. 'Tasman leakage in a fine-
634 resolution ocean model', *Geophysical Research Letters*, 39: n/a--n/a.
635 Walters, D., A. J. Baran, I. Boutle, M. Brooks, P. Earnshaw, J. Edwards, K. Furtado, P. Hi, A. Lock, J. Manners, C.
636 Morcrette, J. Mulcahy, C. Sanchez, C. Smith, R. Stratton, W. Tennant, L. Tomassini, K. Van Weverberg, S.
637 Vosper, M. Willett, J. Browse, A. Bushell, K. Carslaw, M. Dalvi, R. Essery, N. Gedney, S. Hardiman, B.
638 Johnson, C. Johnson, A. Jones, C. Jones, G. Mann, S. Milton, H. Rumbold, A. Sellar, M. Ujiie, M. Whitall,
639 K. Williams, and M. Zerroukat. 2019. 'The Met Office Unified Model Global Atmosphere 7.0/7.1 and
640 JULES Global Land 7.0 configurations', *Geoscientific Model Development*, 12: 1909-63.
641 Yool, A., E. E. Popova, and T. R. Anderson. 2013. 'MEDUSA-2.0: an intermediate complexity biogeochemical
642 model of the marine carbon cycle for climate change and ocean acidification studies', *Geoscientific Model*
643 *Development*, 6: 1767--811.

644